*Am J Physiol Endocrinol Metab* 308: E688–E698, 2015.
First published February 24, 2015; doi:10.1152/ajpendo.00504.2014.

# Loss of survival factors and activation of inflammatory cascades in brain sympathetic centers in type 1 diabetic mice

**Ping Hu,[1] Jeffrey S. Thinschmidt,[2] Sergio Caballero,[2] Samuel Adamson,[1] Louise Cole,[3] Tailoi Chan-Ling,[1]* and Maria B. Grant[4]***

[1]*Department of Anatomy, School of Medical Sciences, Bosch Institute, The University of Sydney, Camperdown, New South Wales, Australia;* [2]*Department of Pharmacology and Therapeutics, University of Florida, Gainesville, Florida;* [3]*Advanced Microscopy Facility, Bosch Institute, School of Medical Sciences, The University of Sydney, Camperdown, New South Wales, Australia; and* [4]*Department of Ophthalmology, The Eugene and Marilyn Glick Eye Institute, Indiana University, Indianapolis, Indiana*

Submitted 7 November 2014; accepted in final form 13 February 2015

**Hu P, Thinschmidt JS, Caballero S, Adamson S, Cole L, Chan-Ling T, Grant MB.** Loss of survival factors and activation of inflammatory cascades in brain sympathetic centers in type 1 diabetic mice. *Am J Physiol Endocrinol Metab* 308: E688–E698, 2015. First published February 24, 2015; doi:10.1152/ajpendo.00504.2014.—Neuroinflammation and neurodegeneration have been observed in the brain in type 1 diabetes (T1D). However, little is known about the mediators of these effects. In T1D mice with 12- and 35-wk duration of diabetes we examined two mechanisms of neurodegeneration, loss of the neuroprotective factors insulin-like growth factor I (IGF-I) and IGF-binding protein-3 (IGFBP-3) and changes in indoleamine 2,3-dioxygenase (IDO) expression in the brain, and compared the response to age-matched controls. Furthermore, levels of matrix metalloproteinase-2 (MMP-2), nucleoside triphosphate diphosphohydrolase-1 (CD39), and ionized calcium-binding adaptor molecule 1 (Iba-1) were utilized to assess inflammatory changes in astrocytes, microglia, and blood vessels. In the diabetic hypothalamus (HYPO), we observed 20% reduction in neuronal soma diameter ($P < 0.05$) and reduced neuronal expression of IGFBP-3 ($-32\%$, $P < 0.05$) and IGF-I ($-15\%$, $P < 0.05$) compared with controls at 35 wk. In diabetic HYPO, MMP-2 expression was increased in astrocytes (46%, $P < 0.01$), and IDO$^+$ cell density rose by (62%, $P < 0.05$). CD39 expression dropped by 30% ($P < 0.05$) in microglia and blood vessels. With 10 wk of systemic treatment using minocycline, an anti-inflammatory agent that crosses the blood-brain barrier, MMP-2, IDO, and CD39 levels normalized ($P < 0.05$). Our results suggest that increased IDO and early loss of CD39$^+$ protective cells lead to activation of inflammation in sympathetic centers of the CNS. As a downstream effect, the loss of the neuronal survival factors IGFBP-3 and IGF-I and the neurotoxic products of the kynurenine pathway contribute to the loss of neuronal density observed in the HYPO in T1D.

diabetes; inflammation; brain; sympathetic nervous system

IN DIABETES, HYPERGLYCEMIA LEADS TO ACTIVATION of metabolic signaling pathways such as protein kinase C (PKC), the polyol pathway, and the advance glycation end products poly(ADP)-ribose polymerase (PARP) and hexosamine. Activation of these pathways leads to an increase in oxidative stress that in turn drives inflammation and cell death (51). This sequence of changes has been observed not only in target organs of diabetic microvascular complications such as the retina, kidney, and nerves but also in the brain, including the hippocampus (43) and the hypothalamus (HYPO) (38). The hyperosmolality associated with new-onset type 1 diabetes (T1D) triggers an increase in neuronal activity and vasopressin production within the hypothalamus. However, after 6 mo of diabetes, an increase in the appearance of small hyperchromatic neurons, a decrease in neuronal density with increases in cleaved caspase-3, TUNEL staining of neurons, and microglial hypertrophy and condensation is observed (38).

Neurons, microglia, and astrocytes constitute the major cellular elements in the HYPO, and activation of these cells is observed along with neuronal degeneration in T1D rats (38, 46). IGF-I and IGF-binding protein-3 (IGFBP-3) comprise critical components of the IGF system that regulate key aspects of cell growth, motility, differentiation, and survival in both normal and pathological conditions. In the central nervous system (CNS), IGF-I enhances neuronal metabolism (4) and modulates neuronal excitability (11). IGF-I also has antiapoptotic (12), antioxidant, and anti-inflammatory roles (28). Therefore, the IGF system has a key role in protecting neurons against insults. IGFBP-3$^+$ neurons are found in both mouse and human HYPO (29), and exogenous administration of IGFBP-3 can protect neurons from apoptosis.

CD39, or nucleoside triphosphate diphosphohydrolase-1, is a transmembrane protein present on the surface of a variety of cells, including microglia, vascular endothelial cells, and leukocytes (33, 47). CD39 hydrolyzes adenosine triphosphate (ATP) and adenosine diphosphate (ADP) to the monophosphate form (AMP) (23). Thus ATP-dependent processes are affected by CD39. Endothelial CD39 plays a critical role in preventing prothrombotic and proinflammatory effects within the vasculature and controls leukocyte trafficking between the blood circulation and tissues (53). CD39 activity can attenuate microglia phagocytosis (5) and migration (19). Mice deficient in CD39 are highly susceptible to streptozotocin (STZ)-induced diabetes, with a rapid rate of onset of diabetes and a 100% incidence (13). In contrast, CD39 overexpression has protective effects against STZ-induced diabetes in mice (14).

Matrix metalloproteinase-2 (MMP-2), one of the many zinc-dependent endopeptidases, functions primarily to mediate the degradation or remodeling of the extracellular matrix and has been implicated in the pathogenesis in diabetes (34). MMP-2 can impact blood-retinal barrier integrity through its disruption of tight-junction proteins such as occludins (25). Increased MMP-2 activity facilitates apoptosis of retinal capillary cells and can contribute to neovascularization associated with end-stage diabetic retinopathy (39, 40).

* T. Chan-Ling and M. B. Grant (senior authors) contributed equally to this article.

Address for reprint requests and other correspondence: M. B. Grant, The Eugene and Marilyn Glick Eye Institute, Univ. of Indiana, Indianapolis, IN 46202 (e-mail: mabgrant@iupui.edu).

Indoleamine 2,3-dioxygenase (IDO) is the first and rate-limiting enzyme of tryptophan catabolism through the kynurenine pathway (KP) (54). The KP represents the major catabolic route of tryptophan and is a source of nicotinamide adenine nucleotide, a cofactor in cellular respiration and energy production that plays a central role in DNA repair and transcriptional regulation (1). In addition, IDO plays a key role in regulation of inflammation. IDO can regulate immune responses and create immune tolerance, acting as a protective feedback mechanism against a possible overshooting T cell response (1). IDO expression is low in normal CNS but increases greatly during inflammatory conditions (1). Proinflammatory cytokines and molecules, especially interferon-γ, increase IDO expression (41). With the increases in IDO expression, the KP downstream products, e.g., quinolinic acid (QUIN), typically rise and have direct effects on neuronal toxicity.

The aim of our study was to examine changes in IGF-I and IGFBP-3 and in IDO expression over time in the brains of T1D mice. Inflammatory changes were assessed using CD39 and MMP-2 as markers. In the T1D mice, we also examined the impact of treatment with minocycline, a tetracycline derivative that crosses both the blood-brain barrier and has anti-inflammatory, antiapoptotic, and antioxidant effects on early inflammatory changes in the brain.

## MATERIALS AND METHODS

*Animals.* Male C57/BJ6 mice were obtained from The Jackson Laboratory (Bar Harbor, ME) and housed in the institutional animal care facilities at the University of Florida. All animals were treated in accordance with the *Guiding Principles in the Care and Use of Animals* [National Institutes of Health (NIH)] and the Association for Research in Vision and Ophthalmology Statement for the Use of Animals in Ophthalmic and Vision Research. All experiments were approved by the Institutional Animal Care and Use Committee of the University of Florida.

*Experimental diabetes.* C57BL/6J mice (The Jackson Laboratory, Bar Harbor, ME) aged 7–10 wk were rendered diabetic with five consecutive daily intraperitoneal injections of STZ (55 mg/kg) freshly dissolved in citrate buffer (pH 4.5). Development of diabetes (defined by blood glucose >250 mg/dl) was verified 1 wk after the first STZ injection (Glucometer Elite XL; Bayer, Elkhart, IN). Glycemic control was estimated on multiple occasions from the measurement of glycohemoglobin (GHb) using either a GHb assay (Glyc-Affin; Perkin-Elmer, Norton, OH) or a glycohemoglobin assay (Helena Glyco Tek Laboratory, Beaumont, TX). A minimum of four animals were examined for each time point. A second group of animals were fed either minocycline-supplemented chow (1 g/kg) or control chow (Purina Mills, Gray Summit, MO) beginning at 14 days following the induction of T1D and then euthanized 10 wk later (12-wk duration of diabetes mellitus).

*Tissue processing.* After confirmed diabetes of 12 and 35 wk duration, T1D animals and age-matched controls were deeply anesthetized and perfused intracardially with phosphate-buffered saline (PBS) followed by 4% paraformaldehyde in 0.1 M phosphate buffer. Brains were immersion-fixed in 4% paraformaldehyde overnight, followed by cryoprotection in 20% sucrose-PBS, and mounted in optimum cutting temperature compound. Serial cross-sections of brains were cut on a cryostat (20 μm thick) and mounted.

*Immunofluorescence histochemistry.* Sections on slides were stained with Iba-1 (Wako, Osaka, Japan) for visualization of microglia/macrophages (50), CD39 (AF4398 for mouse retina; R & D Systems, Minneapolis, MN) for visualization of resident microglia and blood vessels, ZymedS-100β (18-0046; Zymed, Mulgrave, Victoria, Australia) for astrocyte soma, glial fibrillary acidic protein antibody (GFAP; GA5) (Sigma, St. Louis, MO) for astrocyte processes, MMP-2 (Abcam, MA), IDO (LS-B1746; LSBio), IGF-I (220, kind gift from Prof. Robert Baxter and Dr. Sue Firth, Kolling Institute, St. Leonards, New South Wales, Australia), IGFBP-3 (Acris), Neuronal Nuclei (NeuN, MAB 377; Chemicon, Temecula, CA) for neurons, and biotinylated *Griffonia simplicifolia* (*Bandeiraea*) isolectin B4 (GS lectin; Sigma-Aldrich) for endothelial cells and activated microglia/macrophages. The tissues were washed and transferred to secondary antibodies conjugated with either Alexa Fluor 594 or Alexa Fluor 488 (Invitrogen-Molecular Probes, Carlsbad, CA).

*Confocal microscopy.* Imaging was carried out using a Zeiss LSM 510 Meta confocal microscope at the Bosch Advanced Microscopy Facility (University of Sydney). Images were captured with the Zeiss LSM 510 acquisition software (Carl Zeiss). Z-stack images were collected. The optimal interval, pinhole size, and optical depth parameters were consistently maintained as required for the 10 × 0.3, 20 × 0.8, 40 × 0.75, 63 × oil 1.4, and 100 × oil 1.4 NA objectives using an image frame size of 1,024 × 1,024 pixels. The laser lines were 405, 488, 561, and 633 nm. Scan speed and averaging remained consistent for all image capturing in each experiment for both qualitative and quantitative purposes. Image analysis was performed using LSM 510 Meta 4.2 (Carl Zeiss) offline software and Adobe Photoshop CS5 version 12.0 software (Adobe Systems, San Jose, CA) on an Apple Macintosh computer.

*Quantitative analysis of Iba-1$^+$ microglia and NeuN$^+$ neuron size.* Confocal images of the HYPO were analyzed to obtain Iba-1$^+$ microglia and NeuN$^+$ neuron soma size (63–100× images). In each animal, three images were taken from different sections (random 12–24 cells for each mouse), and the images were analyzed using ImageJ software (NIH Research Services Branch; http://rsb.info.nih-.gov/ij/index.html).

*Quantitative analysis of Iba-1$^+$ microglia/macrophage, CD39$^+$ resident microglia, S-100$^+$/MMP-2$^+$/IDO$^+$ astrocyte, and NeuN$^+$/IGF-I$^+$ neuron densities.* The densities of Iba-1$^+$ microglia/macrophage, CD39$^+$ resident microglia, MMP-2$^+$ astrocytes, and NeuN$^+$/IGF-I$^+$ neurons were examined in the HYPO. For each region or tissue, three or more images were taken from different sections for analysis. The positive cells were determined by their specific antibody labeling and unique morphology; for example, MMP-2$^+$ astrocytes had star-shaped morphology. The density of positive cells was quantified manually using ImageJ software. S-100$^+$ astrocytes were counted directly under a microscope at ×20 in different focal planes in the same areas.

*Quantitative analysis of CD39, IGF-I, and IGFBP-3 intensity of immunolabeling.* All images in this study were generated using identical settings for each experiment. For CD39 fluorescence intensity, at least three confocal images (×10) were taken from four or more samples in each group (>12 images in each group). The average fluorescence intensity in the whole area (including CD39$^+$ microglia and blood vessels) of each image was measured using ImageJ software. For IGF-I$^+$ and IGFBP-3$^+$ cell fluorescence intensity, at least three confocal images (×40–100) were taken from four or more samples in each group. In each image, 3–4 IGF-I$^+$ or IGFBP-3$^+$ cells were analyzed using ImageJ software.

*Statistical analysis.* To account for variation, the density or fluorescence intensity of positive cells was normalized by dividing by the mean values of age-matched controls in the same region or tissue and expressed as the percentage of relative densities or fluorescence intensity for each animal. All data are shown as means ± SE. Statistical differences between two groups, for example, control compared with T1D or T1D compared with T1D with minocycline treatment, were determined by applying one-tailed Student's *t*-tests for unpaired groups with equal variance. A $P$ value of $<0.05$ ($P < 0.05$) was considered to be statistically significant.

## RESULTS

*Iba-1$^+$ cells show microglial activation in the HYPO of T1D mice.* The hypothalamus of T1D mice (Fig. 1*B*) with 35 wk of T1D were examined for Iba-1-labeled microglia. The microglia showed significantly larger soma diameters and increased varicosities in their process fields, with many small Iba-1$^+$/GS lectin$^+$ granules. These Iba-1$^+$ granules often contacted and/or surrounded DAPI$^+$ nuclear debris, indicating that Iba-1$^+$ microglia may have been phagocytosing nuclear debris, which is indicative of microglial activation. Age-matched controls showed microglia with smaller, round soma with ramified processes typical of resting microglia (Fig. 1*A*). Quantitative analysis also showed that the Iba-1$^+$ soma was enlarged (44.42 ± 1.47 vs. 38.04 ± 1.14 μm$^2$, $P < 0.05$) in diabetic HYPO.

*CD39 expression on resident microglia and blood vessels is reduced in the 12-wk T1D mice and is restored with minocycline.* In control HYPO, CD39$^+$ microglia somas and blood vessels were stained brightly (Fig. 2*A*); all CD39$^+$ microglia were Iba-1$^+$, and ~99% Iba-1$^+$ microglia were CD39$^+$ (Fig. 2*B*). In contrast in T1D mice with 12-wk diabetes duration, CD39 expression on microglia and blood vessels was reduced by 30% ($P = 0.0019$; Fig. 2*C* compared with control in Fig. 1*A*; Fig. 2*G* shows quantification of fluorescence intensity), whereas the density of CD39$^+$ cells decreased only ~10% (56.0 ± 4.0 in control vs. 50.6 ± 1.6/mm$^2$ in diabetic, $P = 0.07$). Double-labeling indicated that ~50% of Iba-1$^+$ cells also showed reduced CD39$^+$ expression. Approximately 5% of the Iba-1$^+$ cells showed no CD39$^+$ expression (arrowheads in Fig. 2, *C* and *D*). These Iba-1$^+$/CD39$^-$ cells were always located near blood vessels, suggesting that the cells entered from the bloodstream and thus were likely bone marrow-derived cells.

Previously, we showed that the density of Iba-1$^+$ cells in diabetic HYPO returned toward control levels with 10 wk of minocycline treatment (30). We extend these studies by examining the changes in CD39 expression in the minocycline-treated T1D mice. Fluorescence intensity of CD39 increased ~15% in the HYPO of minocycline-treated T1D mice compared with diabetic mice without treatment (Fig. 2, *E* vs. *C*). Figure 2*G* shows the quantitative plots of CD39 expression (control vs. diabetic, $P = 0.0019$; control vs. diabetic + minocycline, $P = 0.021$; diabetic vs. diabetic + minocycline, $P = 0.028$).

*Increased S-100$^+$ astrocyte density and GFAP$^+$ expression in the HYPO and granular insular cortex in 35-wk T1D mice.* The HYPO and granular insular cortex (GIC; Fig. 3, *B*, *D*, and *F*) are regions modulated by the sympathetic nervous system. S-100β$^+$/GFAP$^+$ astrocytes in these regions of 35-wk T1D mice became hypertrophic and exhibited bright and thick GFAP$^+$ processes compared with controls. These astrocytic changes occurred in the same regions where microglia activation was most intense. Quantitative analysis of relative S-100β$^+$ cell density (Fig. 3*G*) shows that diabetic brains had a higher number of S-100β$^+$ cells in the HYPO (358.1 ± 18.1 cells in diabetic vs. 291.2 ± 8.3/mm$^2$ cells in control, $P = 0.0049$) and GIC (density: 244 ± 16.1 cells in diabetic vs. 192 ± 20.2 cells/mm$^2$ in control, $P = 0.0159$) compared with control brains. This latter effect was apparent in regions such as the HYPO and GIC that are modulated by the sympathetic nervous system but not in other regions such as the basal nuclear region (115.2 ± 12.3 cells in diabetic vs. 99.8 ± 4.3 cells/mm$^2$ in control, $P = 0.1366$).

*MMP-2$^+$ expression is increased in cells of HYPO of T1D mice and is reduced with minocycline.* MMP-2 can be expressed by astrocytes and microglia (45) and on blood vessels following stimulation with inflammatory cytokines (27). Stellate MMP-2$^+$ astrocytes were observed to be distributed unevenly across control mouse brain sections. In the HYPO, MMP-2$^+$ cells were more prominent in the periventricular region (Fig. 4*A*), with the density of MMP-2$^+$ cells being 91.0 ± 6.6/mm$^2$ in control HYPO. Double-labeling with MMP-2 and GFAP showed that ~98% of MMP-2$^+$ cells were GFAP$^+$ astrocytes (Fig. 3, *A* and *B*), which confirmed previous studies (35). GS isolectin B4 (*GS* lectin) plus microglia and blood vessels were MMP-2 negative (data not shown).

In the HYPO of 12-wk diabetic mice, the density of MMP-2$^+$ cells increased to 133.3 ± 11.4/mm$^2$ (compared with control, $P = 0.009$; Fig. 4, *C* and *G*). Approximately 95% MMP-2$^+$ cells were GFAP positive (Fig. 4, *C* and *D*), whereas 5% of MMP-2$^+$ cells were GFAP negative (Fig. 4, *C* and *D*, arrows). Minocycline treatment restored the density of MMP-2$^+$ cells to control levels (90.5 ± 12.4/mm$^2$; compared with control, $P = 0.48$; compared with diabetic, $P = 0.03$, Fig. 3, *E–G*).

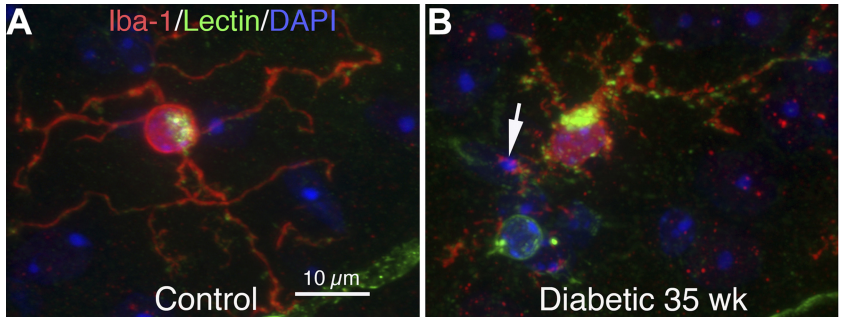


Fig. 1. ionized calcium-binding adaptor molecule 1 (Iba-1)$^+$ microglial activation in the hypothalamus (HYPO) of type 1 diabetic (T1D) mice at 35 wk. *A* and *B*: HYPO region of mouse brain sections triple-stained with Iba-1 (red), GS-lectin (green), and 4,6-diamidino-2-phenylindole (DAPI; blue). *A*: in controls, Iba-1$^+$ microglia had smaller, round somas with long, ramified processes that showed weak GS lectin staining (green). *B*: in diabetic HYPO, the somas of Iba-1$^+$ microglia were larger than that of the controls and showed a marked increase in GS lectin$^+$ activity. Microglia in diabetic HYPO had short and thicker processes, and the processes became more complex and armed with numerous small Iba-1$^+$/GS lectin$^+$ spots. These Iba-1$^+$ granules often contacted and/or surrounded DAPI$^+$ (blue) nuclear debris (arrow), indicating that Iba-1$^+$ microglia may phagocytose nuclear debris.

*Increased IDO$^+$/GFAP$^+$ astrocyte density in the HYPO of T1D mice is mitigated by minocycline.* Weak IDO$^+$ expression was seen on GFAP$^+$ astrocytes in control HYPO (Fig. 5, *A* and *B*). In contrast with the HYPO of T1D mice with 12-wk duration of diabetes (Fig. 5, *C* and *D*), IDO$^+$/GFAP$^+$ cells were increased in number and brightness. Minocycline treatment in diabetic mice (Fig. 5, *E* and *F*) returned the density and brightness of IDO$^+$/GFAP$^+$ astrocytes to control levels. Quantitative analysis (Fig. 5*G*) showed that the IDO$^+$ cell density was significantly higher ($P < 0.05$) in diabetic HYPO (176.1 ± 3.4) compared with control (109.0 ± 6.9) or T1D mice treated with minocycline (108.6 ± 3.7).

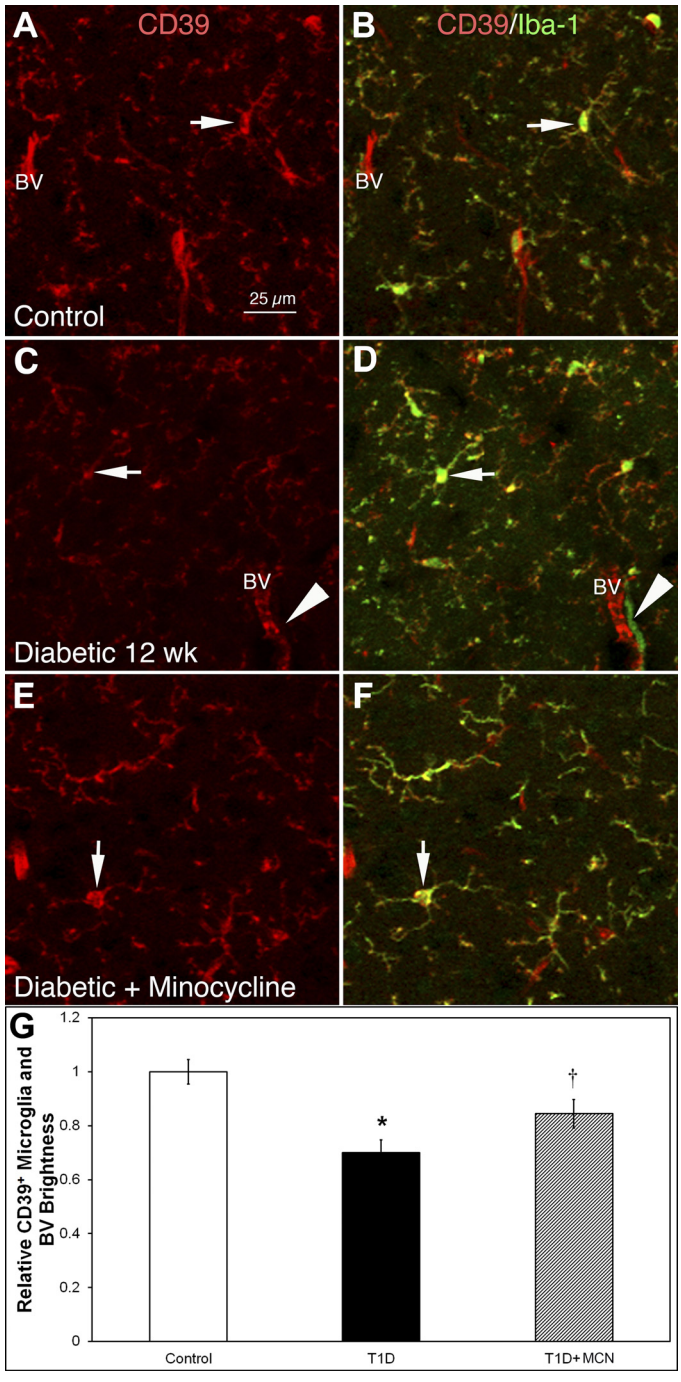


*IGF-I$^+$ immunoreactivity is decreased in NeuN$^+$ neurons of 35-wk T1D HYPO mice.* In controls, IGF-I$^+$ cells were distributed evenly throughout the HYPO (Fig. 6*A*). All IGF-I$^+$ cells were NeuN$^+$ neurons (Fig. 6, *A–C*). In the 35-wk diabetic HYPO (Fig. 6, *D–F*), IGF-I$^+$ cells showed reduced density (431.8 ± 28.0 in diabetic vs. 504.4 ± 7.8/mm$^2$ in control, $P = 0.023$) and intensity of IGF staining (Fig. 6, *A* vs. *D*).

The density of NeuN$^+$ neurons in the diabetic HYPO was similar to that of the control group (1,244.1 ± 2.2/mm$^2$ in control and 1,250.7 ± 2.8/mm$^2$ in diabetic; Fig. 6, *B* vs. *E*). However, increased numbers of NeuN$^+$/IGF-I$^-$ neurons were observed in the diabetic HYPO (compare Fig. 6, *C* and *F*) compared with control HYPO. Higher-power confocal images showed that IGF-I$^+$ was localized to granules in both the control (Fig. 6*G*) and diabetic HYPO (Fig. 6*J*).

In the 35-wk diabetic HYPO, IGF-I$^+$ granules in NeuN$^+$ neurons and IGF-I immunoreactivity was decreased (Fig. 6, *G–I* compared with *J–L*). The size of NeuN$^+$ neurons was also reduced in diabetic HYPO (compare Fig. 6, *H* and *K*). Quantitative analysis showed that the density of IGF-I$^+$ cells decreased in the HYPO at both 12 (448.0 ± 31.6 cells in control vs. 382.4 ± 14.5/mm$^2$ in diabetic, $P = 0.0.048$) and 35 wk (see above) postinduction of diabetes (Fig. 6*M*). However, minocycline treatment in the T1D mice with 12-wk duration of diabetes did not increase the IGF-I$^+$ cell density (409.2 ± 17.8/mm$^2$, $P = 0.138$ with diabetic; Fig. 6*M*).

The size of NeuN$^+$ neurons was 84.8 ± 7.1 μm$^2$ in control but was reduced to 69.7 ± 6.3 μm$^2$ in 35-wk diabetic mice ($P = 0.011$) (Fig. 6*N*). Quantitative analysis showed a 15% loss of IGF-I fluorescence intensity at 35 wk postinduction ($P = 0.03$) but not at 12 wk postinduction (Fig. 6*O*).

*Reduction of IGFBP-3 fluorescence intensity in neurons in the HYPO of 35-wk but not 12-wk T1D mice.* Cells stained for the prosurvival factor IGFBP-3 were widely distributed across the control brain sections, including the HYPO (Fig. 7*A*), GIC (images not shown), and basal nucleus (BN) region (Fig. 7*C*). In the 35-wk diabetic brain (Fig. 7, *B* and *D*), IGFBP-3$^+$ immunoreactivity was reduced by more than 32% ($P = 0.006$) in HYPO (Fig. 7, *A* vs. *B*) but not in BN ($P = 0.477$; Fig. 7,

Fig. 2. Iba-1$^+$ cell density increased, whereas CD39 fluorescence intensity on microglia and blood vessels (BV) was reduced in the HYPO in 12-wk T1D mice. These changes were mitigated by treatment with minocycline. *A–F*: HYPO region of mouse brain sections double-stained with CD39 (red) and Iba-1 (green). *A* and *B*: control animals. *C* and *D*: diabetic mice at 12 wk postinduction. *E* and *F*: diabetic mice treated with minocycline at 12 wk postinduction. CD39 staining in each of the respective groups is shown in *A*, *C*, and *E*, whereas CD39/Iba-1 double labeling is shown in *B*, *D*, and *F*. In controls (*A* and *B*), CD39 was expressed on microglia and BV (*A*); double-labeling (*B*) shows that all CD39$^+$ cells in controls were Iba-1 positive (arrows in *A* and *B* indicate a double-labeled cell). At 12 wk postinduction of diabetes (*C* and *D*), CD39 expression on microglia-like cells and BV was reduced in fluorescence intensity (*C*); double-labeling (*D*) shows some Iba-1$^+$ cells without CD39 expression (arrowheads in *C* and *D*; arrows in *C* and *D* indicate Iba-1$^+$ cells lacking CD39 expression). With minocycline treatment in diabetic mice (*E* and *F*), CD39 expression on microglia-like cells and BV was recovered (*C*). *F*: Iba-1$^+$ cells were reduced in density (arrows in *E* and *F* indicate the same cell). *G*: quantitative analysis shows that the relative fluorescent intensity of CD39$^+$ cells decreased significantly (*$P < 0.001$) in diabetic brains (black bar) compared with control (open bar). With minocycline treatment, the relative fluorescent intensity of CD39$^+$ cells became significantly higher (†$P < 0.03$) than in diabetic brains (gray bar compared with black bar) but was still significantly lower than in control brains (gray bar compared with open bar) (†$P < 0.03$). Calibration in *A* applies to *A–F*.

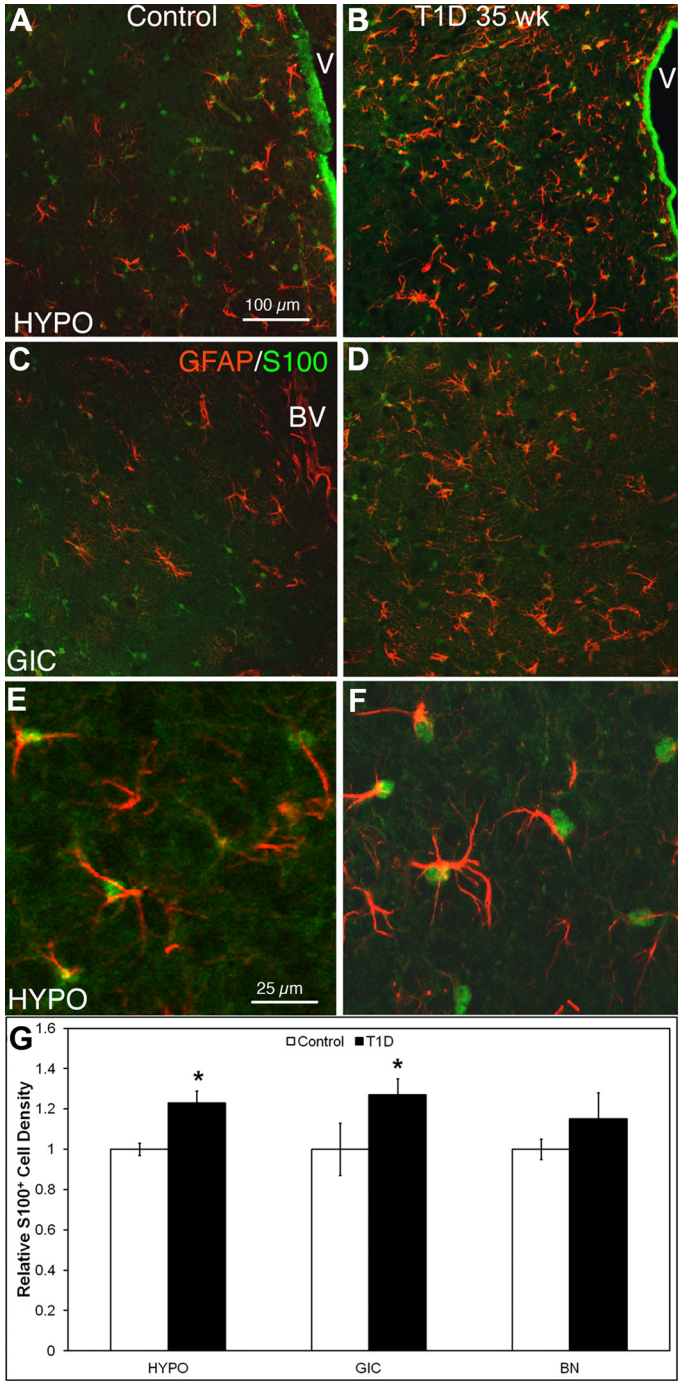


Fig. 3. Astrocytes were activated in the HYPO and granular insular cortex (GIC) of 35-wk T1D mice. Antibodies against both GFAP and S-100β were applied to HYPO and GIC mouse brain sections to visualize astrocytes in control and T1D mice at 35 wk. Both glial fibrillary acidic protein (GFAP) and S-100β visualize astrocyte morphology; S-100β predominantly stains astrocyte somas (green), whereas GFAP visualizes cytoskeletal filament proteins within the cytoplasm (red). *A–D*: regions at low magnification, demonstrating a markedly higher density of astrocytes in T1D at 35 wk in these regions. *E* and *F*: HYPO at higher magnification, confirming that all astrocytes express both GFAP and S-100β. *G*: relative quantitative analysis of $GFAP^+/S\text{-}100\beta^+$ astrocyte cell density in 3 regions of the brain showed that in the 35-wk diabetic HYPO (*B* and *F*) and GIC (*D*) (central nervous system regions connected with the bone marrow), astrocytes showed a significantly ($*P < 0.05$) increased density compared with control brains; however, there was no significant difference evident in the basal nucleus (BN; a region of the brain that is not connected to the bone marrow). Scale bar in *A* applies to *A–D*. Scale bar in *E* applies to *E* and *F*. V, 3rd ventricle.

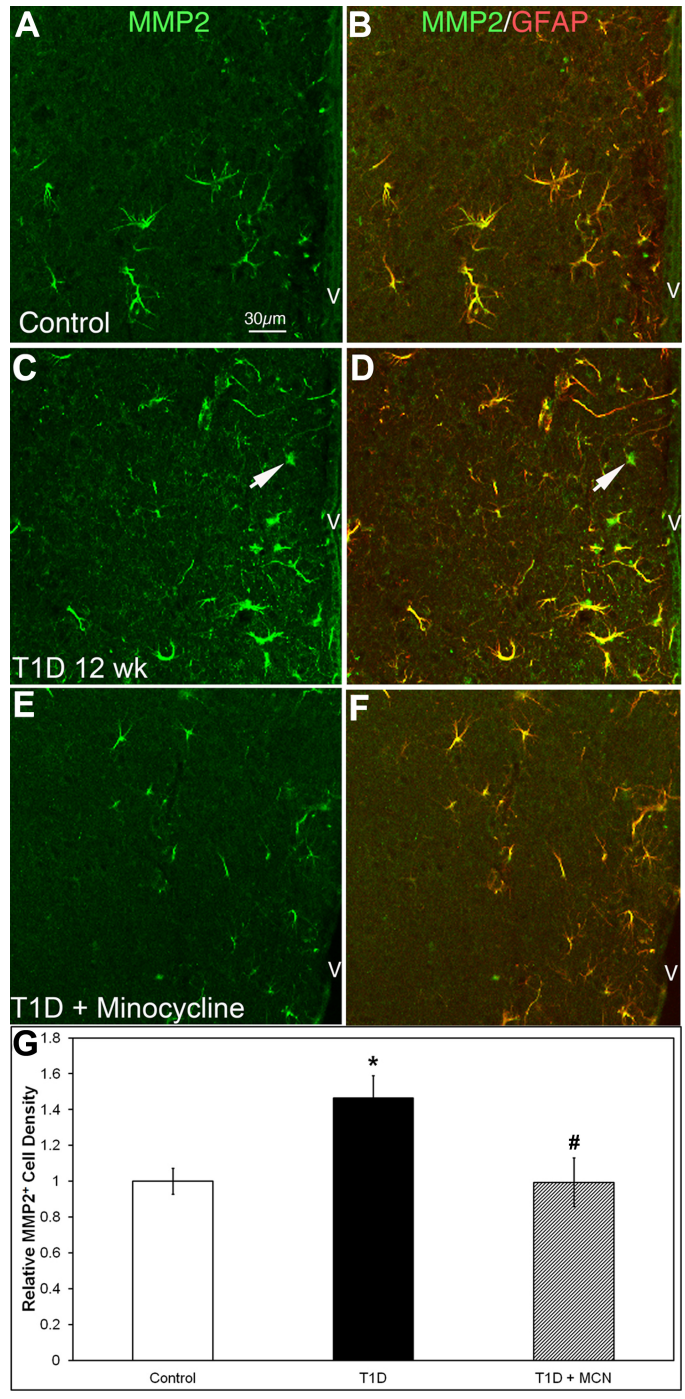


Fig. 4. Matrix metalloproteinase-2 $(MMP\text{-}2)^+/GFAP^+$ cell density was increased in the HYPO in 12-wk T1D mice, and minocycline mitigated MMP-2 expression. *A–F*: HYPO region of mouse brain sections double-stained with MMP-2 (green) and GFAP (red). In controls (*A* and *B*), almost all $MMP\text{-}2^+$ cells were $GFAP^+$ astrocytes. In the 12-wk diabetic HYPO (*C* and *D*), $MMP\text{-}2^+$ cells increased in number and fluorescent intensity, whereas some $MMP\text{-}2^+$ cells were GFAP negative (arrows). With minocycline treatment in diabetic mice (*E* and *F*), the density and fluorescent intensity of $MMP\text{-}2^+$ cells returned to control levels. *G*: relative quantitative analysis shows that the $MMP\text{-}2^+$ cell density was higher in diabetic brains (black bar) compared with controls (open bar; 133.3 ± 11.4 vs. 91.0 ± 6.6/mm$^2$; $*P = 0.009$) and T1D with minocycline treatment (gray bar; 133.3 ± 11.4 vs. 90.5 ± 12.4/mm$^2$; $\#P = 0.03$). There was no significant difference between control and T1D with minocycline treatment (91.0 ± 6.6 vs. 90.5 ± 12.4/mm$^2$, $P = 0.48$). Calibration in *A* applies to *A–F*.

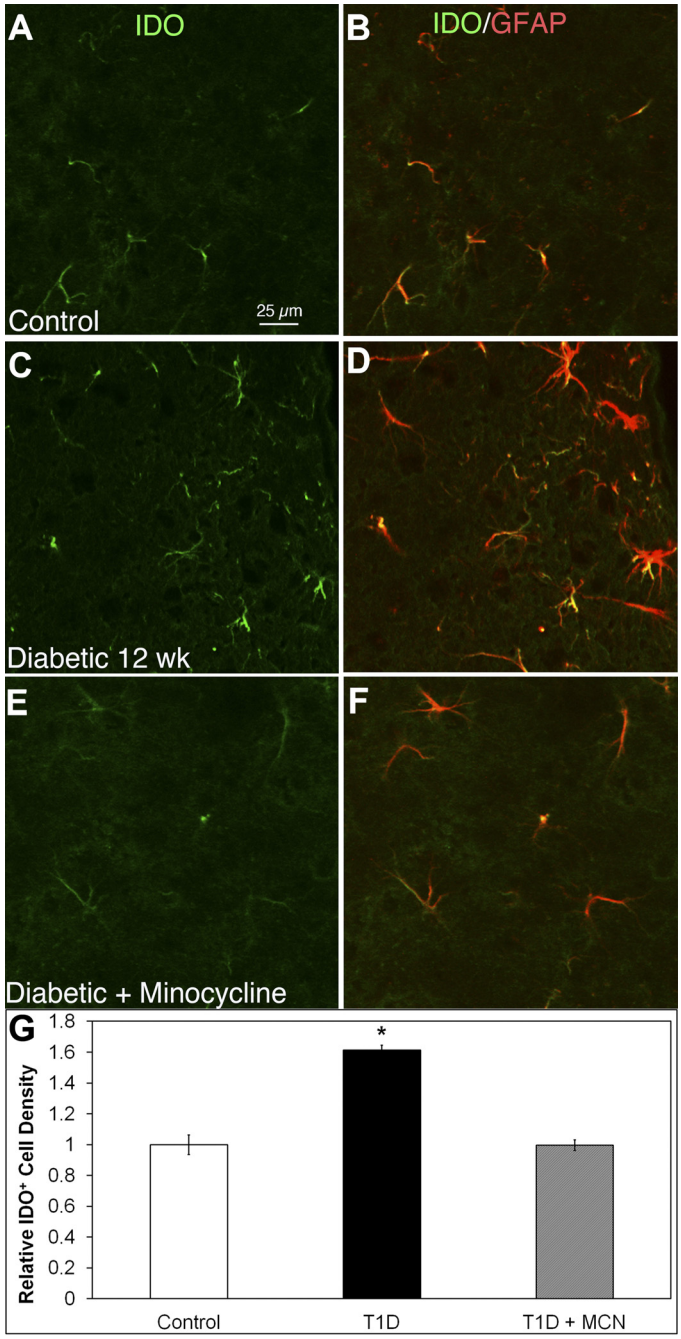


Fig. 5. Indoleamine 2,3-dioxygenase (IDO) expressed in GFAP$^+$ astrocytes increased in density in 12-wk diabetic HYPO, and minocycline (MCN) mitigated IDO expression. *A–F*: HYPO region of mouse brain sections double-stained with IDO (green) and GFAP (red). In controls (*A* and *B*), almost all IDO$^+$ cells were GFAP$^+$ astrocytes. In the 12-wk diabetic HYPO (*C* and *D*), IDO$^+$ cells increased in number and brightness. With minocycline treatment in diabetic mice (*E* and *F*), the density and brightness of IDO$^+$ cells returned to control levels. *G*: relative quantitative analysis showed that the density of IDO$^+$ astrocytes was significantly ($P < 0.05$) higher in diabetic HYPO (black bar) (176.1 ± 3.4) compared with controls (open bar) (109.0 ± 6.9). However, treatment of T1D animals with minocycline (gray bar) resulted in no statistical difference in IDO expression observed between control and minocycline-treated T1D animals, (109.0 ± 6.9 vs. 108.6 ± 3.7, respectively). Calibration in *A* applies to *A–F*.

*C* vs. *D*). High-resolution confocal images showed that IGFBP-3$^+$ cells contained many IGFBP-3$^+$ granules in both the control (Fig. 6*E*) and diabetic HYPO (Fig. 7*F*). These IGFBP-3$^+$ granules were located mostly within NeuN$^+$ neurons (Fig. 7, *E* and *F*). Some IGFBP-3 granules were apparent in between neurons expressing IGFBP-3, suggesting that the IGFBP-3$^+$ produced in these cells is released into the surrounding extracellular space. There were more IGFBP-3$^+$ granules both within the cells and in the extracellular space of controls (Fig. 7*E*) than of diabetics (Fig. 7*F*). The quantitative data show that IGFBP-3 fluorescence intensity was reduced in HYPO (see above) and GIC (30%, $P = 0.032$) but not in BN (see above; Fig. 7*G*). The decrease in IGFBP-3$^+$ immunoreactivity occurred in 35-wk but not 12-wk postinduction (Fig. 7*H*), and minocycline treatment during the first 3 mo of diabetes did not change the levels of IGFBP-3, implying that the loss of IGFBP-3 in neurons is a later event in diabetes.

## DISCUSSION

The major findings of this study include that in T1D the HYPO exhibits *1*) a reduction in CD39$^+$ expression on resident microglia and blood vessels; *2*) an increase in S-100β$^+$ astrocyte density and GFAP$^+$ expression, suggesting diabetes induced astrocyte activation; *3*) increased MMP-2$^+$ and IDO$^+$ expression in astrocytes, further supporting astrocyte activation; and *4*) a decrease in IGF-I$^+$ and IGFBP-3$^+$ immunoreactivity in NeuN$^+$ neurons with fewer IGF-I$^+$ neurons at 35 wk of T1D; and also *5*) that the changes observed in Iba, S-100β, IGF-I, and IGFBP-3 at 35 wk were limited to the expression of regions associated with sympathetic regulation, specifically the HYPO and the GIC.

Metabolic pathways associated with the shunting of excess glucose are known to generate hyperglycemia-induced tissue damage. The polyol pathway, activated during hyperglycemia, leads to consumption of NADPH and depletion of glutathione, which lower the threshold for intracellular oxidative injury. Increased formation of advanced glycation end products damages endothelial cells, thus contributing to vascular damage. Diacylglycerol activation of PKC during hyperglycemia reduces blood flow and increases vascular permeability. Increased shunting of glucose into the hexosamine pathway leads to increased proteoglycan and *O*-linked glycoprotein synthesis. PARP activation, a downstream effector of oxidant-induced DNA damage, is an obligatory step in functional and metabolic changes in the diabetes (52). With time, activation of these metabolic pathways contributes to the pathogenesis of vascular and end-organ damage (Fig. 8). Metabolic activity within these pathways does not depend on neuronal activity and represents a neurologically "passive" response to high glucose conditions.

A critical question remains. Do neurons serve only as end-organ targets of the disease process in diabetes, or do they also actively drive the pathogenesis of end-organ damage? Previously, we sought to address this question and examined the infiltration of bone marrow cells into centers modulated by the sympathetic nervous system, such as the GIC and the HYPO. We found both an increase in the number of infiltrating cells and a change in their activation state. Not surprisingly, this in turn was accompanied by an increase in activation of resident microglia. Using GFP chimeric mice to track bone marrow cell extravasation from the circulation into the hypo-

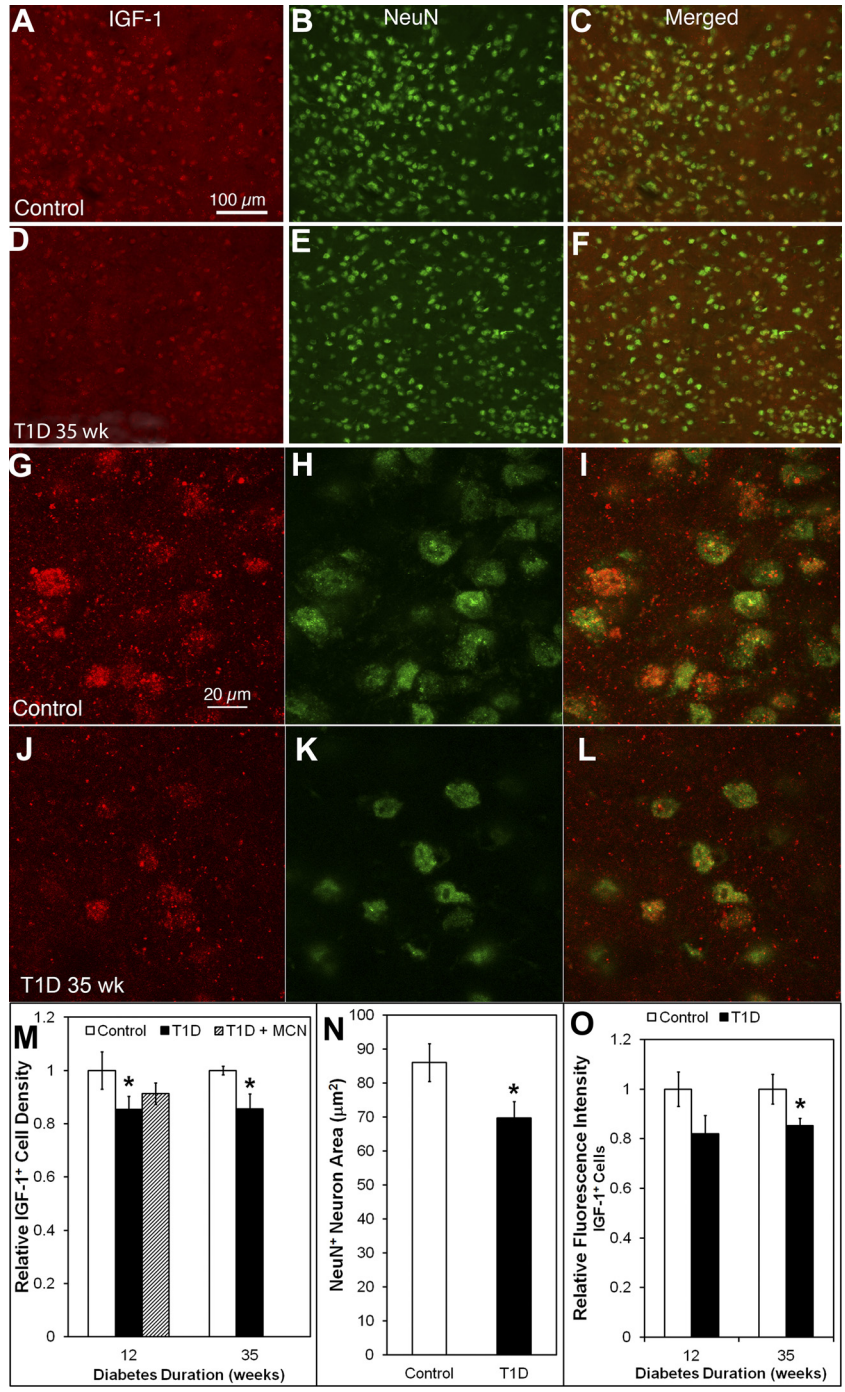


Fig. 6. IGF-I$^+$ neurons decreased in density and fluorescence intensity, and neuronal nuclei (NeuN)$^+$ neurons were reduced in size in the 35-wk diabetic HYPO, but IGF-I$^+$ expression was only partially affected in 12-wk T1D HYPO. *A–L*: HYPO of mouse brain sections double-stained with IGF-I (red) and NeuN (green). IGF-I$^+$ cells were widely distributed in the control HYPO (*A*). In the diabetic HYPO (*D*), IGF-I$^+$ cells decreased in density and fluorescence intensity. All IGF-I$^+$ cells were also NeuN$^+$ neurons in both control (*A–C*) and diabetic animals (*D–F*). NeuN$^+$ cell densities were similar in control and diabetes (compare *B* with *E*); however, NeuN$^+$/IGF-I$^-$ neurons were increased in diabetic HYPO compared with control HYPO (compare *C* with *F*, where there is an increase in NeuN$^+$/IGF-I$^-$ cells in *F*). In the higher magnification (*G–I*), IGF-I$^+$ cells consisted of IGF-I$^+$ granules in the control (*G*) and diabetic HYPO (*J*) and a population of IGF-I$^+$/NeuN$^+$ neurons (*G–L*). In the diabetic HYPO, NeuN$^+$ neurons were reduced in size (compare *H* with *K*; quantitative data in *N*) and had fewer IGF-I$^+$ granules (compare *I* with *L*; quantitative data in *O*). *M*: relative quantitative analysis shows that the density of IGF-I$^+$ neurons decreased in HYPO at both 12 and 35 wk postinduction. There was no difference between control and T1D with minocycline treatment at 12 wk postinduction. Actual cell density nos. and *P* value are given in the text. *N*: quantitative analysis of the size of NeuN$^+$ neurons in the respective fields of view shows that their area is reduced from 84.8 $\pm$ 7.1 $\mu m^2$ in control to 69.7 $\pm$ 6.3 $\mu m^2$ in diabetic mice. *O*: quantitative analysis of relative fluorescence intensity shows that the IGF-I immunoreactivity decrease was statistically significant within the positive cells at 35 wk postinduction but not at 12 wk postinduction. Calibration in *A* applies to *A–F*; calibration in *G* applies to *G–L*. *$P < 0.05$.

thalamus, we showed that, in diabetic hypothalamus, CD45$^+$/CCR2$^+$/GR-1$^+$/Iba-1$^+$ bone marrow-derived monocytes invaded retina, brain, and kidney (30) and that CCL2 and IL-1β mRNA were significantly increased. These studies are in agreement with Luo et al. (46), who showed that, in diabetic hypothalamus, OX42$^+$, or CD11b$^+$, microglia increase. These results collectively suggest that the increased microglia/macrophages in diabetic hypothalamus belonged mainly to the M1 microglia/macrophage lineage.

In this study, we sought to further examine possible mediators responsible for this increased extravasation and activation. The loss of CD39 reactivity selectively seen in the vasculature of the HYPO and GIC would result in facilitated adhesion and subsequent extravasation of inflammatory cells into these specific regions. Critical to extravasation is the expression of proteases by the migrating leukocytes. The increase in MMP-2 expression observed could support increased extravasation of monocytes into the CNS. Similarly, the increase in activation of astrocytes observed in the brains of the diabetic mice would facilitate blood-brain barrier leakage and monocyte extravasation.

Hypothalamic inflammation has been observed in obesity and involves microglia and astrocyte activation and increased expression of TNFα, IL-1β, and IL-6 (7, 8, 24). Although

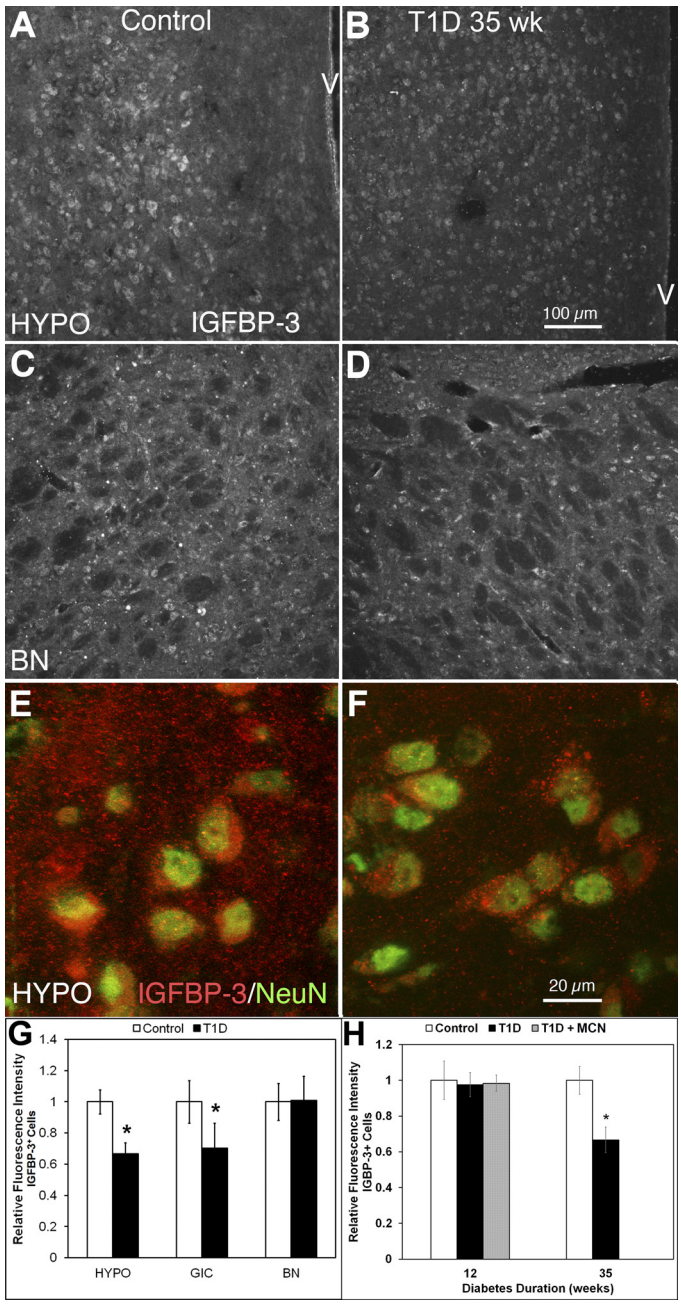


Fig. 7. Fluorescence intensity of IGF-binding protein-3 (IGFBP-3)$^+$ neurons was decreased in the HYPO of 35 wk T1D; however, this change was not observed at 12 wk. Furthermore, an increase in IGFBP-3 fluorescence intensity was also observed in the GIC but not in the BN. *A* and *B*: HYPO of mouse brain sections single-stained with IGFBP-3. Compared with control (*A*), IGFBP-3$^+$ neurons decreased in fluorescence intensity at 35 wk postinduction of diabetes (*B*). *C* and *D*: BN of mouse brain sections single-stained with IGFBP-3. This pair of images shows that there is no significant difference in IGFBP-3$^+$ neuron fluorescence intensity between control (*C*) and diabetic 35-wk mice (*D*) in BN. *E* and *F*: HYPO of mouse brain sections double-stained with IGFBP-3 (red) and NeuN (green). The higher-power images show that NeuN$^+$ neurons contained a greater number of IGFBP-3$^+$ granules in control (*E*), and a large amount of these IGFBP-3$^+$ granules were in the interneuronal space. In the 35-wk postinduction diabetic HYPO (*F*), both the amount of IGFBP-3$^+$ granules within the neurons and the intercellular space between the cells was reduced (compare *E* with *F*). *G*: quantitative analysis showed that the IGFBP-3 fluorescence intensity was decreased at 35 wk ($*P < 0.05$) but not at 12 wk postinduction (data not shown). *H*: quantitative analysis showed that decreased IGFBP-3 fluorescence intensity was seen in HYPO and GIC but not in the BN at 35 wk postinduction. Calibration in *B* applies to *A*–*D*; calibration in *F* applies to *E* and *F*.

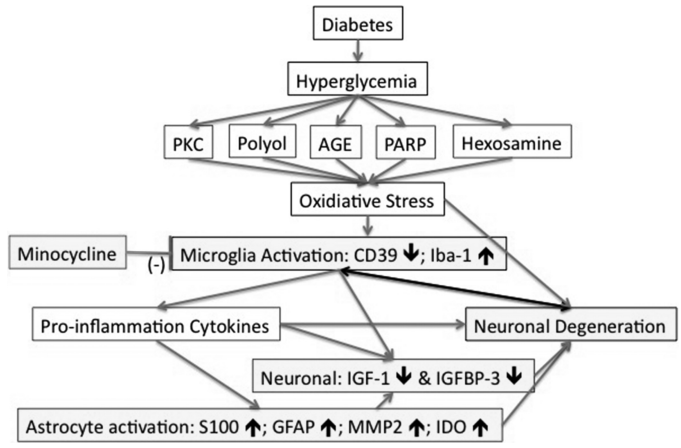


Fig. 8. Interconnections of hypothalamic inflammation in T1D. In T1D, hyperglycemia-induced biochemical alterations drive oxidative stress and lead to the activation of microglia and astrocytes, vascular changes, and neuronal degeneration. In T1D HYPO, most microglia observed displayed an enlarged soma and a mildly activated morphology (Fig. 1). Iba-1$^+$ microglia/macrophages increase in density (30), whereas Iba-1$^+$/CD39$^+$ resident microglia displayed a reduced CD39 fluorescence intensity compared with controls (see Fig. 2). CD39 fluorescence intensity on BV was also reduced in T1D (see Fig. 2). S-100$^+$/GFAP$^+$/MMP2$^+$/IDO$^+$ astrocytes in T1D HYPO increased in density (see Figs. 3–5). The fluorescence intensity of IGF-I and IGFBP-3 on neurons decreased (see Figs. 6 and 7), possibly because of an increased expression of MMP-2 and IDO on astrocytes. In contrast, the fluorescence intensity of c-fos on neurons increased (30). Activated microglia and astrocytes in T1D HYPO could produce proinflammatory cytokines, i.e., cysteine chemokine ligand 2 (CCL2) (30). Proinflammatory cytokines, increased IDO, and loss of IGF-I and IGFBP-3 resulted in neuronal degeneration (Fig. 5*N*), which may further contribute to hypothalamic inflammation in T1D. PKC, protein kinase C; AGE, advanced glycation end product; PARP: poly(ADP-ribose) polymerase.

hypothalamic inflammation has been less well studied in T1D, it has been seen in STZ-induced T1D rats and is accompanied by both microglia and astrocyte activation, and neuronal degeneration (38, 45, 46).

In our study, all CD39$^+$ microglia were Iba-1 positive in both control and diabetic HYPO (Fig. 2, *A*–*D*), suggesting that these microglia were resident cells and not derived from the bone marrow. CD39 is expressed only on resident microglia, and thus CD39$^+$ reactivity is able to distinguish resident microglia from infiltrating bone marrow-derived macrophages (6). In control HYPO, the CD39$^+$ cells had a similar density to Iba-1$^+$ cells (Fig. 2, *A* and *B*). In the diabetic HYPO, the density of CD39$^+$ microglia did not change, but their CD39 immunoreactivity was reduced compare (Fig. 2*C* with Fig. 2*A*; quantitative data are shown in Fig. 2, *G* and *F*). Some Iba-1$^+$ cells were without CD39 labeling (arrows in Fig. 2, *C* and *D*), suggesting that these were derived from the blood (bone marrow derived) and had extravasated from the circulation. As expected, these cells were often found alongside the CD39$^+$ blood vessels. The increased number of Iba-1$^+$/CD39$^-$ cells in the diabetic HYPO suggests that the invading macrophages/monocytes were bone marrow-derived rather than resident macrophages, which is consistent with our previous report (30). This also suggests that bone marrow-derived macrophages can be identified by using CD39/Iba-1 double-labeling and would not require generation of bone marrow chimeras with GFP, which would facilitate the examination of these cells and their behavior in human tissues.

We observed a reduction in CD39 expression in T1D that would typically result in a decrease in adenosine. Thus, the beneficial effects of adenosine would be reduced in diabetes. Adenosine reduces inflammation (21) and prevents the development of diabetic retinopathy by augmenting IL-10-induced STAT3 signaling in M2 macrophages (21, 44). In contrast, increased extracellular ATP contributes to the progression of inflammation in diabetic retinas by activation of the $P2X_7$ receptor (56). Thus, when CD39 expression and activity are reduced, ATP levels will rise and adenosine levels will fall, promoting inflammation, which supports our hypothesis and the results.

CD39 activity also attenuates microglia phagocytosis and migration (5, 19). Endothelial CD39 plays a critical role by terminating the prothrombotic and proinflammatory effects of circulating ATP and ADP, thus tightly regulating hemostasis to prevent excessive clot formation. Blood flow distribution and oxygen delivery are regulated by circulating ATP released by erythrocytes (18). Thus, loss of endothelial CD39 could reduce blood flow and promote hypoxia in the diabetic HYPO.

During acute hypoxia and inflammation associated with T1D, cellular ATP release may promote excessive inflammatory responses that contribute to altered endothelial barrier function and promote leukocyte adhesion and transmigration in affected areas (53, 61). With the loss of CD39, increased ATP levels can induce cell death (42). Reductions in CD39 expression on blood vessels in T1D HYPO may allow bone marrow-derived macrophages to invade more easily. Reducing CD39 expression on resident microglia facilitates activation when bone marrow-derived monocytes invade.

Expression and activity of MMP-2 are elevated in patients with T1D (34) and T2D (55). Increased MMP-2 expression in retina and vitreous (40) is also seen in individuals with diabetic retinopathy. MMP-2 facilitates the apoptosis of retinal capillary cells via damaging the mitochondria (49). Relevant to this study is that the enhanced expression of MMP-2 (Fig. 3) promotes cell death and when expressed by monocytes/macrophages promotes their migration and inflammation and may cleave IGFBP-3 (22).

IDO can play a role in the regulation of inflammation. In mammals, IDO (58) is expressed in macrophages, endothelial cells, neurons, and astrocytes (3). Interferon-γ (IFNγ) is an essential factor for the induction of IDO; however, many other proinflammatory cytokines such as TNFα and IL-1β can also enhance IDO expression (3, 9). In support of this, we previously showed increased IFNγ and IL-1β mRNA in the diabetic HYPO (30). In the brain, enhanced IDO expression increases production of neurotoxins such as QUIN and 3-hydroxyanthranic acid to lead to neurodegeneration (41).

Microglial activation, invasion of bone marrow-derived cells, astrocyte activation, and increased MMP-2 expression occurred only in specific regions such as the HYPO and GIC but not in the BN of T1D brain. This selective localization of activated microglia suggests unique features of these regions of the brain. Our studies would suggest that centers that are modulated by the sympathetic nervous system may exhibit more neuronal damage than other regions of the brain in diabetes due to the selective infiltration of the bone marrow-derived cells and subsequent activation of resident microglia.

To support this contention, it is known that neurons in the HYPO change their morphology and molecular expression in response to chronic stress (26). HYPO neurons in diabetic animals can undergo degeneration (46), showing distension of rough endoplasmic reticulum, swollen mitochondria, and enhanced electron density of their cytoplasm (17). Neurons in the diabetic HYPO show increased arginine, oxytocin, *N*-methyl-D-aspartate receptor 1, neuronal nitric oxide synthase (NOS), and vasopressin expression but downregulated expression of GluR2/3 (20, 46). Both hyperglycemia and hyperosmolality trigger increased neuronal activity (38). Although we observed similar neuron numbers in both control and diabetic HYPO (Fig. 4*G*), neuron size was reduced (compare Fig. 4, *H* and *K*) in T1D and is consistent with the neuronal shrinkage observed by Klein et al. (38).

Expression of IGFBP-3 and IGF-I was reduced in the HYPO neurons (Figs. 6 and 7), whereas c-Fos expression in HYPO neurons was increased in the diabetic mice (30). IGF-I is produced by all neurons in the CNS (15), including developing and adult hypothalamic neurons (16). IGF-I enhances neuron metabolism (4), modulates neuronal excitability (11), and protects against apoptosis (12), oxidative stress, and inflammation (28). Thus, IGF-I is crucial for protecting neurons against hypoxic-ischemic insults (10). In STZ-induced diabetic rats, the circulation levels of IGF-I dropped more than fourfold 16 days post-STZ induction compared with controls (1), with accompaning reductions in brain IGF-I levels (59). Our findings are in agreement with the studies of Aksu et al. (1), as $IGF\text{-}I^+$ neurons showed decreased density and immunoreactivity in the diabetic HYPO (Fig. 6). Considering the protective roles of IGF-I, the reduced levels observed in the neurons of the diabetic HYPO would make these neurons more vulnerable. Similarly, decreased IGFBP-3 immunoreactivity (Fig. 7) could make neurons more susceptible to damage. Hyperglycemia in STZ-induced diabetes can induce increased basal oxygen consumption, thereby causing hypoxia (2) and promoting neuronal death (60). Previously, we have demonstrated that IGFBP-3 can protect cells from apoptosis during hypoxia (36).

IGFBP-3 has vascular effects, including *1*) stimulation of endothelial NOS activity and increasing nitric oxide (NO) generation via the phosphatidylinositol 3-kinase/Akt signaling pathway by activation of SR-B1 (32), *2*) vasodilatation and mediation of vascular repair by increasing NO generation (37), and *3*) protection of blood-retinal barrier integrity (32). Thus, it could be that loss of IGFBP-3 contributes to the neuronal pathology observed in the HYPO.

Previously, we have shown that minocycline could mitigate the invasion of $CD45^+/CCR2^+/GR\text{-}1^+$ bone marrow-derived monocytes in T1D HYPO (30). Minocycline also reduced the density of $Iba\text{-}1^+$ microglia/macrophages in both the HYPO and retina in T1D. In this study, minocycline corrected CD39 expression in microglia and blood vessels toward control nondiabetic levels. Minocycline reduced GFAP activation in astrocytes and MMP2 expression (Fig. 4). Minocycline can reduce microglial-derived membrane type 1 (MT1)-MMP (48). MT1-MMP is a MMP-2 membrane-bound activator and cleaves inactive pro-MMP-2 into MMP-2 via activation of Toll-like receptors and the p38 mitogen-activated protein kinase (MAPK) pathway (48). Minocycline can block p38 MAPK pathway activation in microglia (57) and represents a therapeutic candidate against inflammation in T1D. The increased expression of Iba-1, MMP-2, and IDO and the reduced

expression of CD39 in the diabetic HYPO were all mitigated by treatment with minocycline.

Our studies provide additional insight into the impact of T1D on the sympathetic centers of the CNS. Infiltration and activation of bone marrow cells that infiltrate sympathetic centers and the accompanying activation of resident microglia are promoted by T1D-induced vascular changes, including loss of CD39 reactivity that can facilitate adhesion and extravasation of bone marrow-derived monocytes into these regions. Critical to their extravasation is the expression of proteases, including MMP-2. The activation of astrocytes in the brain further facilitates blood-brain barrier leakage and leukocyte extravasation. In the brain, enhanced IDO expression increases production of neurotoxins such as QUIN and 3-hydroxyanthranic acid to promote neuronal damage by reducing levels of neuronal protective factors (41). The changes in the blood-brain barrier and in microglia and astrocyte activation may contribute to the loss of the neuronal survival factors IGF-I and IGFBP-3 that is manifested as neuronal degeneration.

Our study would support that diabetes-induced oxidative damage in the CNS can lead to activation of microglia with the subsequent release of inflammatory cytokines. These proinflammatory cytokines in turn can activate astrocytes. Activation of astrocytes results in increased IDO expression, which increases production of neurotoxins (41). This in turn can result in reduced expression of the neuronal protective factors IGF-I and IGFBP-3 (Fig. 8). Use of agents such as minocycline that cross the blood-brain barrier to reduce neuroinflammation may provide a useful addition to the armamentarium of agents used to treat diabetes-induced CNS pathology.

## ACKNOWLEDGMENTS

We thank Drs. Robert Baxter and Sue Firth for the gift of antibodies (Kolling Institute of Medical Research, University of Sydney) and Jane Nappi (University of Florida) and Marda Jorgenson (University of Florida) for their technical assistance. Confocal imaging was carried out at the Bosch Institute Advanced Microscopy Facility at the University of Sydney.

## GRANTS

This work was supported by NIH Grants EY-07739, EY-12601, DK-090730-02, EY-018358, and EY-021626 (M. B. Grant). Additional support was provided by National Health and Medical Research Council of Australia Grants 571100 and 1005730, the Australian Government Department of Innovation, Industry, Science, and Research: International Science Linkages Program Grant CG130097, the Baxter Charitable Foundation, the Alma Hazel Eddy Trust, and the Rebecca L. Cooper Medical Foundation. (TC-L). P. Hu and S. Adamson are Brian M. Kirby Foundation Gift of Sight Initiative Scholarship holders and NWG Macintosh Foundation Grant Awardees. M. B. Grant and T. Chan-Ling are the guarantors of this work, had full access to all of the data, and take full responsibility for the integrity of data and the accuracy of the data analysis.

## DISCLOSURES

No conflicts of interest, financial or otherwise, are declared by the authors.

## AUTHOR CONTRIBUTIONS

P.H., J.S.T., T.C.-L., and M.B.G. conception and design of research; P.H., J.S.T., S.C., S.A., and L.C. performed experiments; P.H., S.C., L.C., and T.C.-L. analyzed data; P.H., J.S.T., S.C., S.A., L.C., T.C.-L., and M.B.G. interpreted results of experiments; P.H. and S.C. prepared figures; P.H., T.C.-L., and M.B.G. drafted manuscript; P.H., J.S.T., S.C., S.A., L.C., T.C.-L., and M.B.G. edited and revised manuscript; P.H., J.S.T., S.C., S.A., L.C., T.C.-L., and M.B.G. approved final version of manuscript.

## REFERENCES

1. **Aksu I, Ates M, Baykara B, Kiray M, Sisman AR, Buyuk E, Baykara B, Cetinkaya C, Gumus H, Uysal N.** Anxiety correlates to decreased blood and prefrontal cortex IGF-1 levels in streptozotocin induced diabetes. *Neurosci Lett* 531: 176–181, 2012.
2. **Alder VA, Su EN, Yu DY, Cringle SJ, Yu PK.** Diabetic retinopathy: early functional changes. *Clin Exp Pharmacol Physiol* 24: 785–788, 1997.
3. **Andre C, O'Connor JC, Kelley KW, Lestage J, Dantzer R, Castanon N.** Spatio-temporal differences in the profile of murine brain expression of proinflammatory cytokines and indoleamine 2,3-dioxygenase in response to peripheral lipopolysaccharide administration. *J Neuroimmunol* 200: 90–99, 2008.
4. **Bondy CA, Cheng CM.** Insulin-like growth factor-1 promotes neuronal glucose utilization during brain development and repair processes. *Int Rev Neurobiol* 51: 189–217, 2002.
5. **Bulavina L, Szulzewsky F, Rocha A, Krabbe G, Robson SC, Matyash V, Kettenmann H.** NTPDase1 activity attenuates microglial phagocytosis. *Purinergic Signal* 9: 199–205, 2013.
6. **Butovsky O, Siddiqui S, Gabriely G, Lanser AJ, Dake B, Murugaiyan G, Doykan CE, Wu PM, Gali RR, Iyer LK, Lawson R, Berry J, Krichevsky AM, Cudkowicz ME, Weiner HL.** Modulating inflammatory monocytes with a unique microRNA gene signature ameliorates murine ALS. *J Clin Invest* 122: 3063–3087, 2012.
7. **Cai D, Liu T.** Hypothalamic inflammation: a double-edged sword to nutritional diseases. *Ann NY Acad Sci* 1243: E1–E39, 2011.
8. **Calegari VC, Torsoni AS, Vanzela EC, Araujo EP, Morari J, Zoppi CC, Sbragia L, Boschero AC, Velloso LA.** Inflammation of the hypothalamus leads to defective pancreatic islet function. *J Biol Chem* 286: 12870–12880, 2011.
9. **Campbell BM, Charych E, Lee AW, Moller T.** Kynurenines in CNS disease: regulation by inflammatory cytokines. *Front Neurosci* 8: 12, 2014.
10. **Cardona-Gómez GP, Mendez P, DonCarlos LL, Azcoitia I, Garcia-Segura LM.** Interactions of estrogens and insulin-like growth factor-I in the brain: implications for neuroprotection. *Brain Res Brain Res Rev* 37: 320–334, 2001.
11. **Carro E, Nuñez A, Busiguina S, Torres-Aleman I.** Circulating insulin-like growth factor I mediates effects of exercise on the brain. *J Neurosci* 20: 2926–2933, 2000.
12. **Carro E, Trejo JL, Núñez A, Torres-Aleman I.** Brain repair and neuroprotection by serum insulin-like growth factor I. *Mol Neurobiol* 27: 153–162, 2003.
13. **Chia JS, McRae JL, Cowan PJ, Dwyer KM.** The CD39-adenosinergic axis in the pathogenesis of immune and nonimmune diabetes. *J Biomed Biotechnol* 2012: 320495, 2012.
14. **Chia JS, McRae JL, Thomas HE, Fynch S, Elkerbout L, Hill P, Murray-Segal L, Robson SC, Chen JF, d'Apice AJ, Cowan PJ, Dwyer KM.** The protective effects of CD39 overexpression in multiple low-dose streptozotocin-induced diabetes in mice. *Diabetes* 62: 2026–2035, 2013.
15. **D'Ercole AJ, Ye P, Calikoglu AS, Gutierrez-Ospina G.** The role of the insulin-like growth factors in the central nervous system. *Mol Neurobiol* 13: 227–255, 1996.
16. **Daftary SS, Gore AC.** IGF-1 in the brain as a regulator of reproductive neuroendocrine function. *Exp Biol Med (Maywood)* 230: 292–306, 2005.
17. **Dheen ST, Tay SS, Wong WC.** Ultrastructural changes in the hypothalamic paraventricular nucleus of the streptozotocin-induced diabetic rat. *Acta Anat (Basel)* 149: 291–299, 1994.
18. **Ellsworth ML, Sprague RS.** Regulation of blood flow distribution in skeletal muscle: role of erythrocyte-released ATP. *J Physiol* 590: 4985–4991, 2012.
19. **Farber K, Markworth S, Pannasch U, Nolte C, Prinz V, Kronenberg G, Gertz K, Endres M, Bechmann I, Enjyoji K, Robson SC, Kettenmann H.** The ectonucleotidase cd39/ENTPDase1 modulates purinergic-mediated microglial migration. *Glia* 56: 331–341, 2008.
20. **Fernstrom JD, Fernstrom MH, Kwok RP.** In vivo somatostatin, vasopressin, and oxytocin synthesis in diabetic rat hypothalamus. *Am J Physiol Endocrinol Metab* 258: E661–E666, 1990.
21. **Ferrante CJ, Pinhal-Enfield G, Elson G, Cronstein BN, Hasko G, Outram S, Leibovich SJ.** The adenosine-dependent angiogenic switch of macrophages to an M2-like phenotype is independent of interleukin-4 receptor alpha (IL-4Ralpha) signaling. *Inflammation* 36: 921–931, 2013.

22. **Fowlkes JL, Enghild JJ, Suzuki K, Nagase H.** Matrix metalloproteinases degrade insulin-like growth factor-binding protein-3 in dermal fibroblast cultures. *J Biol Chem* 269: 25742–25746, 1994.
23. **Fung CY, Marcus AJ, Broekman MJ, Mahaut-Smith MP.** P2X(1) receptor inhibition and soluble CD39 administration as novel approaches to widen the cardiovascular therapeutic window. *Trends Cardiovasc Med* 19: 1–5, 2009.
24. **García-Cáceres C, Yi CX, Tschöp MH.** Hypothalamic astrocytes in obesity. *Endocrinol Metab Clin North Am* 42: 57–66, 2013.
25. **Giebel SJ, Menicucci G, McGuire PG, Das A.** Matrix metalloproteinases in early diabetic retinopathy and their role in alteration of the blood-retinal barrier. *Lab Invest* 85: 597–607, 2005.
26. **Herman JP, Flak J, Jankord R.** Chronic stress plasticity in the hypothalamic paraventricular nucleus. *Prog Brain Res* 170: 353–364, 2008.
27. **Hernandez-Guillamon M, Martinez-Saez E, Delgado P, Domingues-Montanari S, Boada C, Penalba A, Boada M, Pagola J, Maisterra O, Rodriguez-Luna D, Molina CA, Rovira A, Alvarez-Sabin J, Ortega-Aznar A, Montaner J.** MMP-2/MMP-9 plasma level and brain expression in cerebral amyloid angiopathy-associated hemorrhagic stroke. *Brain Pathol* 22: 133–141, 2012.
28. **Higashi Y, Sukhanov S, Anwar A, Shai SY, Delafontaine P.** IGF-1, oxidative stress and atheroprotection. *Trends Endocrinol Metab* 21: 245–254, 2010.
29. **Honda M, Eriksson KS, Zhang S, Tanaka S, Lin L, Salehi A, Hesla PE, Maehlen J, Gaus SE, Yanagisawa M, Sakurai T, Taheri S, Tsuchiya K, Honda Y, Mignot E.** IGFBP3 colocalizes with and regulates hypocretin (orexin). *PLoS One* 4: e4254, 2009.
30. **Hu P, Thinschmidt JS, Yan Y, Hazra S, Bhatwadekar A, Caballero S, Salazar T, Miyan JA, Li W, Derbenev A, Zsombok A, Tikhonenko M, Dominguez JM 2nd, McGorray SP, Saban DR, Boulton ME, Busik JV, Raizada MK, Chan-Ling T, Grant MB.** CNS inflammation and bone marrow neuropathy in type 1 diabetes. *Am J Pathol* 183: 1608–1620, 2013.
32. **Jarajapu YP, Cai J, Yan Y, Li Calzi S, Kielczewski JL, Hu P, Shaw LC, Firth SM, Chan-Ling T, Boulton ME, Baxter RC, Grant MB.** Protection of blood retinal barrier and systemic vasculature by insulin-like growth factor binding protein-3. *PLoS One* 7: e39398, 2012.
33. **Kaczmarek E, Koziak K, Sevigny J, Siegel JB, Anrather J, Beaudoin AR, Bach FH, Robson SC.** Identification and characterization of CD39/vascular ATP diphosphohydrolase. *J Biol Chem* 271: 33116–33122, 1996.
34. **Kadoglou NP, Daskalopoulou SS, Perrea D, Liapis CD.** Matrix metalloproteinases and diabetic vascular complications. *Angiology* 56: 173–189, 2005.
35. **Khuth ST, Akaoka H, Pagenstecher A, Verlaeten O, Belin MF, Giraudon P, Bernard A.** Morbillivirus infection of the mouse central nervous system induces region-specific upregulation of MMPs and TIMPs correlated to inflammatory cytokine expression. *J Virol* 75: 8268–8282, 2001.
36. **Kielczewski JL, Hu P, Shaw LC, Li Calzi S, Mames RN, Gardiner TA, McFarland E, Chan-Ling T, Grant MB.** Novel protective properties of IGFBP-3 result in enhanced pericyte ensheathment, reduced microglial activation, increased microglial apoptosis, and neuronal protection after ischemic retinal injury. *Am J Pathol* 178: 1517–1528, 2011.
37. **Kielczewski JL, Jarajapu YP, McFarland EL, Cai J, Afzal A, Li Calzi S, Chang KH, Lydic T, Shaw LC, Busik J, Hughes J, Cardounel AJ, Wilson K, Lyons TJ, Boulton ME, Mames RN, Chan-Ling T, Grant MB.** Insulin-like growth factor binding protein-3 mediates vascular repair by enhancing nitric oxide generation. *Circ Res* 105: 897–905, 2009.
38. **Klein JP, Hains BC, Craner MJ, Black JA, Waxman SG.** Apoptosis of vasopressinergic hypothalamic neurons in chronic diabetes mellitus. *Neurobiol Dis* 15: 221–228, 2004.
39. **Kowluru RA, Kanwar M.** Oxidative stress and the development of diabetic retinopathy: contributory role of matrix metalloproteinase-2. *Free Radic Biol Med* 46: 1677–1685, 2009.
40. **Kowluru RA, Zhong Q, Santos JM.** Matrix metalloproteinases in diabetic retinopathy: potential role of MMP-9. *Expert Opin Investig Drugs* 21: 797–805, 2012.
41. **Kwidzinski E, Bechmann I.** IDO expression in the brain: a double-edged sword. *J Mol Med (Berl)* 85: 1351–1359, 2007.
42. **Levesque SA, Kukulski F, Enjyoji K, Robson SC, Sevigny J.** NTPDase1 governs P2X7-dependent functions in murine macrophages. *Eur J Immunol* 40: 1473–1485, 2010.
43. **Li ZG, Zhang W, Grunberger G, Sima AA.** Hippocampal neuronal apoptosis in type 1 diabetes. *Brain Res* 946: 221–231, 2002.
44. **Liou GI, Ahmad S, Naime M, Fatteh N, Ibrahim AS.** Role of adenosine in diabetic retinopathy. *J Ocul Biol Dis Infor* 4: 19–24, 2011.
45. **Lively S, Schlichter LC.** The microglial activation state regulates migration and roles of matrix-dissolving enzymes for invasion. *J Neuroinflammation* 10: 75, 2013.
46. **Luo Y, Kaur C, Ling EA.** Neuronal and glial response in the rat hypothalamus-neurohypophysis complex with streptozotocin-induced diabetes. *Brain Res* 925: 42–54, 2002.
47. **Marcus AJ, Broekman MJ, Drosopoulos JH, Islam N, Pinsky DJ, Sesti C, Levi R.** Metabolic control of excessive extracellular nucleotide accumulation by CD39/ecto-nucleotidase-1: implications for ischemic vascular diseases. *J Pharmacol Exp Ther* 305: 9–16, 2003.
48. **Markovic DS, Vinnakota K, van Rooijen N, Kiwit J, Synowitz M, Glass R, Kettenmann H.** Minocycline reduces glioma expansion and invasion by attenuating microglial MT1-MMP expression. *Brain Behav Immun* 25: 624–628, 2011.
49. **Mohammad G, Kowluru RA.** Matrix metalloproteinase-2 in the development of diabetic retinopathy and mitochondrial dysfunction. *Lab Invest* 90: 1365–1372, 2010.
50. **Nakano K, Migita M, Mochizuki H, Shimada T.** Differentiation of transplanted bone marrow cells in the adult mouse brain. *Transplantation* 71: 1735–1740, 2001.
51. **Obrosova IG, Drel VR, Pacher P, Ilnytska O, Wang ZQ, Stevens MJ, Yorek MA.** Oxidative-nitrosative stress and poly(ADP-ribose) polymerase (PARP) activation in experimental diabetic neuropathy: the relation is revisited. *Diabetes* 54: 3435–3441, 2005.
52. **Obrosova IG, Li F, Abatan OI, Forsell MA, Komjati K, Pacher P, Szabo C, Stevens MJ.** Role of poly(ADP-ribose) polymerase activation in diabetic neuropathy. *Diabetes* 53: 711–720, 2004.
53. **Salmi M, Jalkanen S.** Ectoenzymes controlling leukocyte traffic. *Eur J Immunol* 42: 284–292, 2012.
54. **Schwarcz R, Bruno JP, Muchowski PJ, Wu HQ.** Kynurenines in the mammalian brain: when physiology meets pathology. *Nat Rev Neurosci* 13: 465–477, 2012.
55. **Signorelli SS, Malaponte G, Libra M, Di Pino L, Celotta G, Bevelacqua V, Petrina M, Nicotra GS, Indelicato M, Navolanic PM, Pennisi G, Mazzarino MC.** Plasma levels and zymographic activities of matrix metalloproteinases 2 and 9 in type II diabetics with peripheral arterial disease. *Vasc Med* 10: 1–6, 2005.
56. **Sugiyama T.** Role of P2X7 receptors in the development of diabetic retinopathy. *World J Diabetes* 5: 141–145, 2014.
57. **Suk K.** Minocycline suppresses hypoxic activation of rodent microglia in culture. *Neurosci Lett* 366: 167–171, 2004.
58. **Taylor MW, Feng GS.** Relationship between interferon-gamma, indoleamine 2,3-dioxygenase, and tryptophan catabolism. *FASEB J* 5: 2516–2522, 1991.
59. **Trejo JL, Piriz J, Llorens-Martin MV, Fernandez AM, Bolós M, LeRoith D, Nuñez A, Torres-Aleman I.** Central actions of liver-derived insulin-like growth factor I underlying its pro-cognitive effects. *Mol Psychiatry* 12: 1118–1128, 2007.
60. **Xu M, Zhang HL.** Death and survival of neuronal and astrocytic cells in ischemic brain injury: a role of autophagy. *Acta Pharmacol Sin* 32: 1089–1099, 2011.
61. **Yegutkin GG.** Nucleotide- and nucleoside-converting ectoenzymes: Important modulators of purinergic signalling cascade. *Biochim Biophys Acta* 1783: 673–694, 2008.